Research Square

Preprints are preliminary reports that have not undergone peer review.
They should not be considered conclusive, used to inform clinical practice,
or referenced by the media as validated information.

Reliability and Sensing Analysis of IRS-Assisted NOMA ISAC for IoT Networks

Pramod Kumar Yadav
Indian Institute of Technology BHU
Sonam Jain
sonam.ece@iitbhu.ac.in
Indian Institute of Technology BHU

Research Article

Keywords: Integrated sensing and communication (ISAC), non-orthogonal multiple access (NOMA), intelligent reflecting surface (IRS), base station (BS), outage probability (OP), probability of detection (PoD), Internet of Things (IoT)

Posted Date: November 12th, 2026

DOI: https://doi.org/10.21203/rs.3.rs-11477727/v1

License: This work is licensed under a Creative Commons Attribution 4.0 International License.
Read Full License

Additional Declarations: No competing interests reported.

Reliability and Sensing Analysis of IRS-Assisted NOMA ISAC for IoT Networks

Pramod Kumar Yadav[1] and Sonam Jain[1]

[1*]Department of Electronics Engineering, Indian Institute of Technology (BHU) Varanasi, Varanasi, India.

Contributing authors: pramodkumaryadav.rs.ece22@iitbhu.ac.in; sonam.ece@iitbhu.ac.in;

Abstract

Future intelligent wireless networks require reliable and spectrum-efficient communication while simultaneously supporting environmental sensing. Integrated Sensing and Communication (ISAC) enables this integration through shared wireless resources; however, multiuser communication in dense and blockage-prone environments remains challenging. This paper proposes a full-duplex Intelligent Reflecting Surface (IRS)-assisted Non-Orthogonal Multiple Access (NOMA)-ISAC framework for simultaneous uplink/downlink communication and target sensing. Considering co-channel, self-loop, and target-induced interference, outage probability (OP) and probability of detection (PoD) are derived over Nakagami-$\boldsymbol{m}$ fading channels. The analysis shows that increasing transmit power and IRS elements improves far-user reliability and sensing performance, whereas IRS-enhanced multiuser interference can degrade uplink near-user performance, revealing a fundamental reliability tradeoff. Simulations validate the analysis and demonstrate superior communication and sensing performance over conventional NOMA-ISAC systems. The proposed framework offers a promising solution for reliable and energy-efficient intelligent wireless networks.

Keywords: Integrated sensing and communication (ISAC), non-orthogonal multiple access (NOMA), intelligent reflecting surface (IRS), base station (BS), outage probability (OP), probability of detection (PoD), Internet of Things (IoT).

1 Introduction

Next-generation wireless communication systems demand reliable, spectrum-efficient, and energy-efficient architectures capable of simultaneously supporting wireless communication and environmental sensing for applications such as IoT connectivity, wireless sensor networks, smart-city monitoring, and intelligent infrastructure. This requirement has led to the emergence of Integrated Sensing and Communication (ISAC), in which sensing and communication operations share spectral and hardware resources [1]. The similarities between radar sensing and communication in terms of signal processing techniques, hardware architectures, and channel models provide a fundamental basis for their integration. By jointly utilizing these resources, ISAC can improve spectrum efficiency, reduce deployment costs, and achieve integration gains [2–4]. Accordingly, sensing and communication (S&C) performance analysis and waveform design for ISAC systems employing orthogonal multiple access (OMA) techniques have been widely investigated in [5], [6], and [7].

However, the joint utilization of spectral and hardware resources introduces significant interference between sensing and communication operations, which can degrade both communication reliability and sensing accuracy, particularly in dense intelligent environments [8]. This challenge becomes more pronounced when a large number of IoT devices simultaneously exchange monitoring and safety-critical information. Non-Orthogonal Multiple Access (NOMA) provides an effective approach for addressing this challenge by allowing multiple users to share the same time-frequency resources while improving spectral efficiency [9–14]. Through superposition coding and successive interference cancellation (SIC), NOMA enables flexible resource allocation and efficient multiuser interference management while improving connectivity for weak or distant users [15], [16]. These characteristics make NOMA particularly attractive for massive IoT connectivity and resource-efficient ISAC systems [8].

A NOMA-aided downlink ISAC framework was proposed in [17], demonstrating improved communication–sensing performance compared with conventional OMA schemes. Subsequently, several studies investigated the performance of uplink (UL) and downlink (DL) NOMA-ISAC systems, primarily by considering UL and DL transmission separately [7], [18], [17]. However, practical intelligent wireless networks often require the simultaneous operation of UL and DL IoT devices, resulting in additional mutual interference that can substantially affect both communication reliability and sensing performance. To address this scenario, [19] jointly considered UL and DL users for outage and sensing performance analysis, while [20] investigated full-duplex multi-antenna NOMA systems under finite blocklength transmission.

Despite these advances, the existing NOMA-ISAC studies do not adequately address propagation limitations encountered in dense and blockage-prone environments, such as underground metro stations, tunnels, smart parking areas, and airport terminals. In these environments, the direct communication links can experience severe attenuation or blockage, particularly at high carrier frequencies. Intelligent Reflecting Surfaces (IRSs) provide a promising solution by intelligently reconfiguring the propagation environment through passive beamforming. By creating favorable reflected links, IRS can improve coverage and communication reliability while reducing the required transmit power [21–23]. Therefore, the integration of IRS with NOMA-ISAC offers the potential to jointly address multiuser connectivity, propagation blockage, and energy efficiency.

Several recent studies have investigated IRS-assisted ISAC systems. For example, [24] proposed an IRS-assisted ISAC framework for maximizing the achievable sum rate while satisfying radar sensing requirements. The work in [25] investigated IRS-enabled ISAC-assisted mobile edge computing with the objective of minimizing total energy consumption under sensing and latency constraints. Similarly, [26] studied millimeter-wave IRS-assisted ISAC through the joint optimization of radar waveforms, beamforming, and IRS phase shifts. While these studies demonstrate the potential of IRS for enhancing ISAC performance, they primarily focus on resource optimization, beamforming design, achievable rate, or energy minimization. They do not provide a comprehensive reliability and sensing analysis for an IRS-assisted NOMA-ISAC system in which UL and DL users operate concurrently in the presence of sensing targets and the associated interference.

Accordingly, the novelty of the proposed framework lies in jointly integrating three key functionalities that have largely been investigated separately in the existing literature: (i) IRS-assisted propagation enhancement for overcoming blockage and coverage limitations, (ii) NOMA-based simultaneous multiuser transmission for improved spectral efficiency, and (iii) full-duplex concurrent UL/DL communication integrated with target sensing. Unlike existing IRS-assisted ISAC studies that mainly focus on optimization-based designs, and conventional NOMA-ISAC studies that generally consider either separate UL/DL operation or do not account for IRS-assisted propagation, this work provides a unified reliability and sensing analysis of their combined operation. In particular, the proposed framework explicitly accounts for the interference arising from concurrent communication and sensing operations, including target-induced interference and self-loop interference. Furthermore, the analysis is developed over Nakagami-m fading channels,

thereby enabling the characterization of a broad range of practical propagation conditions.

To the best of the authors' knowledge, the reliability and sensing performance of an IRS-assisted full-duplex NOMA-ISAC system with concurrent UL/DL users and sensing targets over Nakagami-m fading channels have not been comprehensively investigated, as summarized in Table 1. Moreover, unlike conventional central limit theorem (CLT)-based approximations that may become inaccurate when the number of IRS elements is small, this work employs a Laplace transform-based statistical framework to characterize the IRS-assisted channel. This enables the proposed analysis to provide a more appropriate performance characterization across different IRS configurations.

Motivated by these research gaps, this work investigates the communication reliability and sensing performance of an IRS-assisted full-duplex NOMA-ISAC system for intelligent and energy-efficient wireless networks. The major contributions of this work are summarized as follows:

- A full-duplex IRS-assisted NOMA-ISAC framework is proposed to enable simultaneous UL/DL communication and target sensing in blockage-prone intelligent wireless environments.
- Closed-form and approximate expressions for the DL outage probability (OP) are derived under Nakagami-m fading, considering co-channel and target-induced interference for large and small numbers of IRS elements, respectively.
- Approximate expressions for the UL OP are derived using numerical integration by accounting for self-loop, target-induced, and multiuser interference under the NOMA framework.
- The probability of detection (PoD) at the BS is derived by jointly considering the IRS-assisted and direct target echo paths in the presence of UL interference.
- The derived expressions provide insights into the effects of transmit power, the number of IRS elements, interference, and NOMA power allocation on communication reliability and sensing performance, revealing important performance tradeoffs among UL and DL users.
- Analytical results are validated through simulations and demonstrate improved communication reliability and sensing performance compared with conventional NOMA-ISAC systems.

2 System Model

The proposed system model shown in Fig. 1 conciders an ISAC enabled wireless network comprising a full-duplex base station (BS) equipped with a single transmit and receive antenna, which simultaneously performs communication and sensing. The fixed near and far UL/DL users correspond to the respective IoT devices in the considered system. The fixed near and far UL/DL users represent transportation-oriented IoT devices such as roadside sensors, smart parking units, traffic monitoring terminals. The BS operates as a radar transceiver for target detection, while simultaneously receiving UL signals from the UL IoT devices U_1 and U_2, and also simultaneously transmitting the information to DL IoT devices D_1 and D_2. IRS panels are deployed to assist the far UL and DL IoT devices by providing additional reflective paths and intelligently controlling the phase of the reflected signals toward the receiver by using perfect channel state information (CSI) [33]. Hence, improving coverage and reliability in blockage-prone transportation environments such as intersections, tunnels, and urban roads.
We consider the IoT device D_1 as a typical cell-centered device, classified as a near user (N), which communicates directly with the BS without relying on the IRS. On the other hand, the IoT device D_2 is located near the cell edge. It is classified as the far user (F) and relies on the IRS-assisted link to communicate with the BS. The DL channel $h_1 \in \mathbb{C}$ represents the link from the BS to D_1. The channels $\mathbf{g_1}$ and $\mathbf{g_2}$ denote the links from the BS to the IRS and from the IRS to D_2, respectively. The UL channels $h_2 \in \mathbb{C}$, $\mathbf{g_3}$ and $\mathbf{g_4}$ represent the links from U_1 (near user) to the BS, from U_2 (far user) to the IRS and from IRS to BS, respectively. h_{LI} models the loop self interference (LSI) channel generated due to the BS operating in full-duplex mode and distributed as $\mathcal{CN}(0, \sigma_{LI}^2)$. $h_{BS\to T}$ (h_{TBS}) and $h_{T\to BS}$ (h_{BST}) denote the sensing channels between the BS and the target. Furthermore,

Table 1: Comparison with Existing Literature

	[27]	[28]	[29]	[30]	[31]	[19]	[32]	**Proposed Scheme**
Reliability Analysis	✓	✓				✓	✓	✓
Sensing Analysis	✓	✓		✓	✓	✓	✓	✓
IRS aided networks		✓		✓	✓		✓	✓
NOMA aided scheme	✓	✓	✓	✓	✓		✓	✓
UL& DL analysis	✓		✓			✓		✓
Nakagami-m fading channel								✓

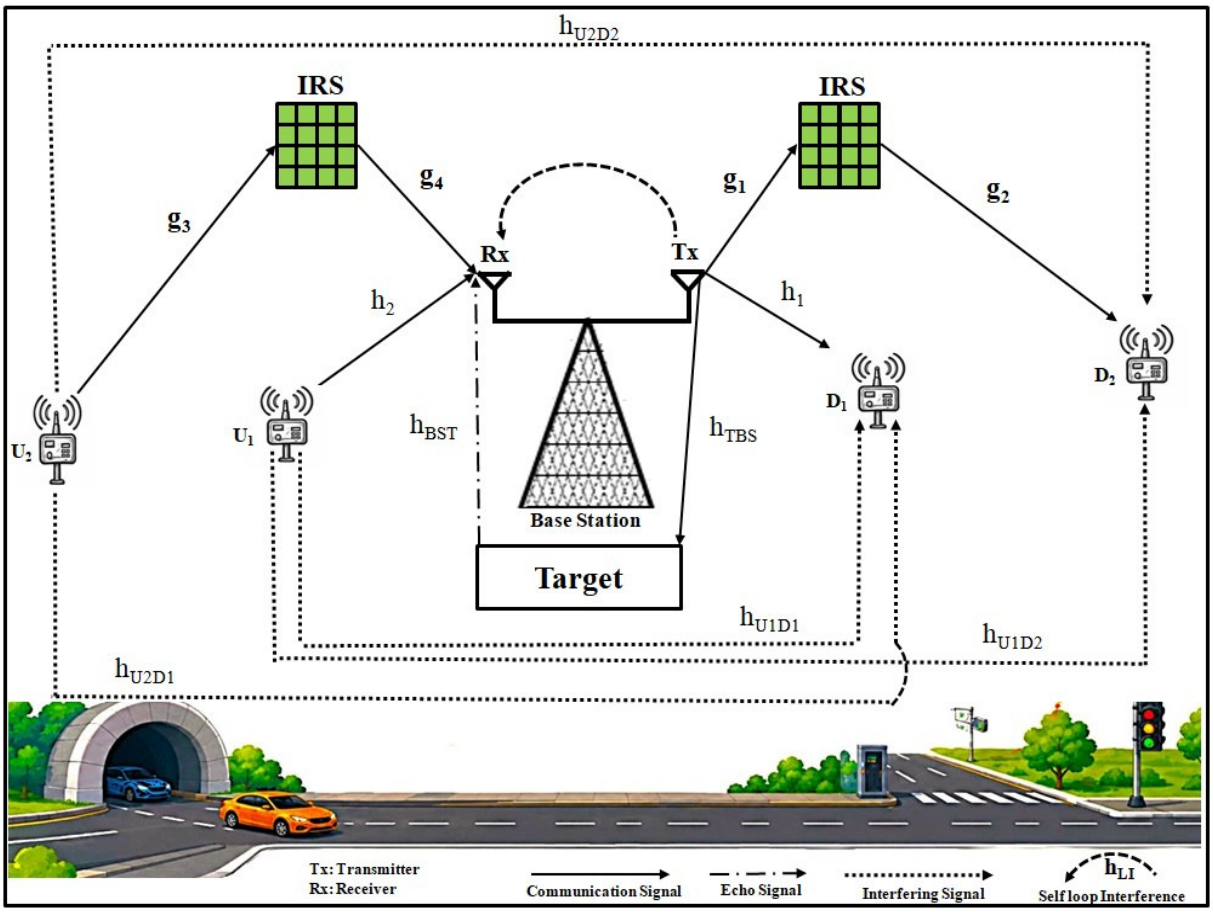


Fig. 1: Proposed System Model.

$h_{U_iD_j} \sim \mathcal{CN}(0, \sigma^2_{U_iD_j})$ denotes the UL-to-DL co-channel interference channel between U_i and D_j, where $i, j \in \{1, 2\}$. The system operates in a simultaneous transmission and reception mode, these links generate co-channel interference in the DL. All the IoT devices share their power according to the power domain NOMA strategy [34]. It is assumed that the direct transmission path between the BS to D_2 is blocked, as depicted in Fig. 1, due to their large separation distance [35],[36]. Additionally, the transceiver is assumed to possess perfect knowledge of CSI.

2.1 Downlink Transmission

For the DL transmission, the signal $x = \sqrt{Pa_1}s_1 + \sqrt{Pa_2}s_2$ comprises both communication and sensing components, enabling the BS to transmit the

data to the paired DL NOMA users while simultaneously detecting the radar target. Where, s_1 and s_2 denote the transmitted symbols. $\sqrt{a_1}$ and $\sqrt{a_2}$ represent the power allocation factor for N and F, respectively. It follows NOMA protocol i.e., $(a_1 + a_2 = 1)$ [34]. The direct link between BS and N experiences severe fading due to significant blockage and modeled as a Rayleigh fading channel, which is denoted by h_1 [35]. The channels $\mathbf{g_1}$ and $\mathbf{g_2}$ between BS-IRS and IRS-D_2 are modeled by a realistic Nakagami-m fading model with fading parameters, m_{g_1} and m_{g_2}, respectively [37]. All communication links are assumed to experience small-scale fading. The received signal at D_1 and D_2 are given by Eqn.1 and Eqn.2, respectively.
where, $\mathbf{g_1} = [g_{11}e^{-i\alpha_1}, g_{12}e^{-i\alpha_2}, \ldots, g_{1K}e^{-i\alpha_K}]$ and $\mathbf{g_2} = [g_{21}e^{-i\beta_1}, g_{22}e^{-i\beta_2}, \ldots, g_{2K}e^{-i\beta_K}]$ denote the channel vectors. The IRS reflection matrix is given by $\mathbf{\Phi} = (\Gamma_1, \Gamma_2, \ldots, \Gamma_K)$, where $\Gamma_k = |\Gamma_k|e^{i\phi_K}$ denotes the reflection coefficient of the k-th element. The parameters $|\Gamma_k|$ and ϕ_k represent its reflection amplitude and phase shift of the k-th reflecting element, respectively. The total number of reflecting elements present in the IRS panel is denoted by K $(1 \leq k \leq K)$. $\epsilon_{D_1} \sim \mathcal{CN}(0, \sigma^2_{\epsilon_{D_1}})$ and $\epsilon_{D_2} \sim \mathcal{CN}(0, \sigma^2_{\epsilon_{D_2}})$ are the sensing to communication interference for D_1 and D_2. U_1 and U_2 are the UL transmitter, they are transmitting their information y_{U_1} and y_{U_2} with the power P_1 and P_2 to the BS, respectively.
The received instantaneous signal to noise ratio (SNR) at D_1 and signal to interference-noise ratio (SINR) at D_2 are γ_N and γ_{D_2} as presented in Eqn.3 and Eqn.4.
It is assumed that all the phases are available at all IRS controller and applying the optimal co-phasing $(\phi_k = \alpha_k + \beta_k)$. n represent additive white Gaussian noise (AWGN). The instantaneous SINR received at D_2 after applying co-phasing is denoted by $\gamma_{_F}$ and expressed in Eqn.5.

2.2 Uplink Transmission

For the UL transmission, the BS receives the signals transmitted by U_1 and U_2, along with the echo signal reflected from the target. Thus, the received signal at the BS is expressed by y_r as represented in Eqn.6. where, $\mathbf{g_3} = [g_{31}e^{-i\alpha_1}, g_{32}e^{-i\alpha_2}, \ldots, g_{3K}e^{-i\alpha_K}]$ and $\mathbf{g_4} = [g_{41}e^{-i\beta_1}, g_{42}e^{-i\beta_2}, \ldots, g_{4K}e^{-i\beta_K}]$. Moreover, $\epsilon_{U_1} \sim \mathcal{CN}(0, \sigma^2_{\epsilon_{U_1}})$, $\epsilon_{U_2} \sim \mathcal{CN}(0, \sigma^2_{\epsilon_{U_2}})$ and δ are the sensing to communication interference for U_1, U_2 and scattering coefficient of the target, respectively. By invoking monostatic reciprocity, the effective sensing channel between the BS and target, accounting for the BS-to-target and target-to-BS propagation paths, is expressed by h_{SS} $(h_{SS} = h_{TBS}\ h_{BST})$. The probability density function (PDF) of $|h_{SS}|^2$ is derived in [38] and expressed as $f_{|h_{SS}|^2(q)}$, as given in Eqn.7. For the UL NOMA analysis, after applying optimal co-phasing, the received SINR of U_1 and the SNR of U_2 at the BS are denoted by γ_{U_1}, γ_{U_2}, and presented in Eqn.8 and Eqn.9, respectively.

$$y_{D_1} = \underbrace{(h_1 + \epsilon_{D_1})x}_{\text{DL Signal for } D_1} + \underbrace{P_1 h_{U_1 D_1} y_{U_1} + P_2 h_{U_2 D_1} y_{U_2}}_{\text{UL to } D_1 \text{ interference}} + n, \tag{1}$$

$$y_{D_2} = \underbrace{(\mathbf{g_1 \Phi g_2}^T + \epsilon_{D_2})x}_{\text{DL Signal for } D_2} + \underbrace{P_1 h_{U_1 D_2} y_{U_1} + P_2 h_{U_2 D_2} y_{U_2}}_{\text{UL to } D_2 \text{ interference}} + n, \tag{2}$$

$$\gamma_N = \frac{a_1 P |h_1|^2}{P\sigma^2_{\epsilon_{D_1}} + P_1 |h_{U_1 D_1}|^2 + P_2 |h_{U_2 D_1}|^2 + \sigma^2}, \tag{3}$$

$$\gamma_{D_2} = \frac{a_2 P \left|\mathbf{g_1 \Phi g_2}^T\right|^2}{a_1 P \left|\mathbf{g_1 \Phi g_2}^T\right|^2 + P\sigma^2_{\epsilon_{D_2}} + P_1 |h_{U_1 D_2}|^2 + P_2 |h_{U_2 D_2}|^2 + \sigma^2}, \tag{4}$$

$$\gamma_{_F} = \frac{a_2 P \left(\sum_{k=1}^{K} |g_{1k}||g_{2k}|\right)^2}{a_1 P \left(\sum_{k=1}^{K} |g_{1k}||g_{2k}|\right)^2 + P\sigma^2_{\epsilon_{D_2}} + P_1 |h_{U_1 D_2}|^2 + P_2 |h_{U_2 D_2}|^2 + \sigma^2}, \tag{5}$$

$$y_r = \underbrace{\left(\mathbf{g_3 \Phi g_4}^T + \epsilon_{U_2}\right) y_{U_2} + (h_2 + \epsilon_{U_1}) y_{U_1}}_{\text{UL Signal}} + \underbrace{(h_{LI} + \delta\ h_{SS}) y_s}_{\text{Echo and LSI}} + n, \tag{6}$$

3 Performance Analysis

In this section, we analyze the reliability and sensing performance of IRS assisted NOMA ISAC system. Specifically, we examine the OP for DL in subsection 3.1, OP for UL in 3.2 and target sensing in 3.3, respectively.

3.1 Downlink OP Analysis

OP indicates the probability that the received signal falls below a specified threshold value and mathematically it is given by P_{out_l} as presented in Eqn.10 where, $l \in [N, F]$. Accordingly, the OP for N denoted by P_{out_N}, is given in Eqn.11. Substituting Eqn.3 into Eqn.11, we obtain Eqn.12, which is further simplified in Eqn.13-14, where $\rho = \frac{P}{\sigma^2}$, $\rho_1 = \frac{P_1}{\sigma^2}$, and $\rho_2 = \frac{P_2}{\sigma^2}$. Here, $Z \in \{h_1, h_{U_1D_1}, h_{U_2D_1}\}$, where, h_1, $h_{U_1D_1}$, and $h_{U_2D_1}$ are denoted by u, w, and v, respectively. The PDF of $|Z|^2$ follows a central chi-square distribution with two degrees of freedom is given by Eqn.15. By substituting the PDF from Eqn.15 into Eqn.14 and solving it, the OP for N is obtained and presented in Eqn.16.

$$f_{|h_{SS}|^2(q)} = \frac{1}{2\sqrt{q}\sigma^2} e^{\frac{-\sqrt{q}}{\sigma^2}}, \tag{7}$$

$$\gamma_{U_1} = \frac{|h_2|^2 P_1}{P_2 \left(\sum_{k=1}^{K} |g_{3k}||g_{4k}|\right)^2 + P_2\sigma^2_{\epsilon_{U_2}} + P_1\sigma^2_{\epsilon_{U_1}} + P(|h_{LI}|^2 + \delta^2|h_{SS}|^2) + \sigma^2}, \tag{8}$$

$$\gamma_{U_2} = \frac{P_2 \left(\sum_{k=1}^{K} |g_{3k}||g_{4k}|\right)^2}{P_1\sigma^2_{\epsilon_{U_1}} + P_2\sigma^2_{\epsilon_{U_2}} + P(|h_{LI}|^2 + \delta^2|h_{SS}|^2) + \sigma^2}, \tag{9}$$

$$P_{out_l} = P_r\left(\log_2(1+\gamma_l) \le R_l\right), \tag{10}$$

$$P_{out_N} = P_r\left(\log_2(1+\gamma_N) \le R_N\right), \tag{11}$$

$$P_{out_N} = P_r\left(\frac{a_1 P|h_1|^2}{P\sigma^2_{\epsilon_{D_1}} + P_1|h_{U_1D_1}|^2 + P_2|h_{U_2D_1}|^2 + \sigma^2} \le 2^{R_N} - 1\right), \tag{12}$$

$$P_{out_N} = P_r\left(|h_1|^2 \le \frac{(2^{R_N}-1)(\rho\sigma^2_{\epsilon_{D_1}} + \rho_1|h_{U_1,D_1}|^2 + \rho_2|h_{U_2,D_1}|^2 + 1)}{a_1\rho}\right), \tag{13}$$

$$P_{out_N} = \int_0^\infty f_{|w|^2}(w) \int_0^\infty f_{|v|^2}(v) \int_0^{B_1} f_{|h_1|^2}(u)\, du\, dv\, dw, \tag{14}$$

$$f_{|Z|^2}(z) = \frac{1}{\mathrm{Var}(Z)} \exp\left(-\frac{z}{\mathrm{Var}(Z)}\right) \tag{15}$$

where, $B_1 = \frac{(2^{R_N}-1)(\rho\sigma^2_{\epsilon_{D_1}} + \rho_1 w + \rho_2 v + 1)}{a_1\rho}$ and Var(.) denotes the variance operator.

$$P_{out_N} = 1 - \frac{(a_1\rho\sigma^2_{D_1})^2 e^{-\frac{(2^{R_N}-1)(\rho\sigma^2_{\epsilon_{D_1}}+1)}{a_1\rho\sigma^2_{D_1}}}}{(a_1\rho\sigma^2_{D_1}+(2^{R_N}-1)\rho_1\sigma^2_{U_1D_1})(a_1\rho\sigma^2_{D_1}+(2^{R_N}-1)\rho_2\sigma^2_{U_2D_1})} \tag{16}$$

The OP for the far user D_2, P_{out_F} is derived by substituting Eqn.5 into Eqn.17 and simplifying the resulting resulting expression, as given in Eqn.19. Following the approach in [39], both sides of Eqn.19 are normalized by dividing them by $K(1-\epsilon)$. This normalization facilitates the approximation of resulting random variable using a standard probability distribution. For a sufficiently large number of reflecting elements K, $T = \frac{\left(\sum_{k=1}^{K}|g_{1_k}||g_{2_k}|\right)^2}{K(1-\epsilon)}$ can be approximated using CLT based approach as presented in Eqn.22. CLT-based approach is valid only for large value of K. In order to deal with small number of IRS elements Laplace transform based approach is used and the pdf of cascaded channel $\sum_{k=1}^{K}|g_{1_k}||g_{2_k}|$ is approximated as expressed in Eqn.24. Where, $\lambda = \frac{K\epsilon}{1-\epsilon}$ and $\epsilon = \frac{1}{m_{g_1}m_{g_2}}\left(\frac{\Gamma(m_{g_1}+0.5)}{\Gamma m_{g_1}}\right)^2\left(\frac{\Gamma(m_{g_2}+0.5)}{\Gamma m_{g_2}}\right)^2$.The power allocation coefficients must satisfy $(a_2 - a_1(2^{R_F}-1)) > 0$ for the feasible NOMA operation. Substituting the PDF into Eqn.21, the OP for the large number of IRS elements $P^l_{out_F}$ is derived and presented in Eqn.23.

$$P_{out_F} = P_r\left(\gamma_F \le 2^{R_F}-1\right), \tag{17}$$

$$P_{out_F} = P_r\left(\frac{a_2P\left(\sum_{k=1}^{K}|g_{1k}||g_{2k}|\right)^2}{a_1P\left(\sum_{k=1}^{K}|g_{1k}||g_{2k}|\right)^2 + P\sigma^2_{\epsilon_{D_2}} + P_1|h_{U_1D_2}|^2 + P_2|h_{U_2D_2}|^2 + \sigma^2} \le 2^{R_F}-1\right), \tag{18}$$

$$P_{out_F} = P_r\left(\left(\sum_{k=1}^{K}|g_{1k}||g_{2k}|\right)^2 \le \frac{(2^{R_F}-1)(P\sigma^2_{\epsilon_{D_2}} + P_1|h_{U_1D_2}|^2 + P_2|h_{U_2D_2}|^2 + \sigma^2)}{P(a_2 - a_1(2^{R_F}-1))}\right), \tag{19}$$

$$P_{out_F} = P_r\left(\frac{\left(\sum_{k=1}^{K}|g_{1k}||g_{2k}|\right)^2}{K(1-\epsilon)} \le \frac{(2^{R_F}-1)(\rho\sigma^2_{\epsilon_{D_2}} + \rho_1|h_{U_1D_2}|^2 + \rho_2|h_{U_2D_2}|^2 + 1)}{\rho(a_2 - a_1(2^{R_F}-1))K(1-\epsilon)}\right), \tag{20}$$

$$P_{out_F} = \int_0^\infty f(w)\int_0^\infty f(v)\int_0^{B_2} f(t)\,dt\,dv\,dw, \tag{21}$$

$$f(t) = \frac{\lambda^{\frac{1}{4}}}{2}e^{-\frac{t+\lambda}{2}}t^{-\frac{1}{4}}I_{-\frac{1}{2}}\left(\sqrt{\lambda t}\right), \tag{22}$$

$$P^l_{out_F} = C_1\Bigg[\gamma(i+0.5, C_2) + \frac{1}{C_3-1}e^{\frac{C_2(C_3+C_4-C_3C_4)}{C_3C_4}}\left(\frac{C_3C_4}{C_3+C_4}\right)^{i+0.5} \times \Gamma\left(i+0.5, \frac{C_2(C_3+C_4)}{C_3C_4}\right) - \frac{e^{\frac{C_2}{C_4}}}{(C_3-1)}\left(\frac{C_4}{C_4+1}\right)^{i+0.5}\Gamma\left(i+0.5, \frac{C_2(C_4+1)}{C_4}\right)\Bigg] \tag{23}$$

where,

$$B_2 = \frac{(2^{R_F}-1)(\rho\sigma^2_{\epsilon_{D_2}} + \rho_1 w + \rho_2 v + 1)}{\rho(a_2 - a_1(2^{R_F}-1))K(1-\epsilon)}.$$

$$C_1 = e^{-\lambda/2}\sum_{i=0}^{\infty}\left(\frac{\lambda}{2}\right)^i \frac{1}{i!\Gamma(i+0.5)},$$

$$C_2 = \frac{(2^{R_F}-1)(\rho\sigma^2_{\epsilon_{D_2}} + 1)}{2K(1-\epsilon)\rho\,(a_2 - a_1(2^{R_F}-1))},$$

$$C_3 = \frac{(2^{R_F}-1)\rho_1\sigma^2_{U_1D_2}}{2K(1-\epsilon)\rho\,(a_2 - a_1(2^{R_F}-1))},$$

$$C_4 = \frac{(2^{R_F}-1)\rho_2\sigma^2_{U_2D_2}}{2K(1-\epsilon)\rho\,(a_2 - a_1(2^{R_F}-1))}.$$

$$f(\psi) = \frac{\widetilde{m}^K}{\Gamma(2m_sK)}\psi^{2m_sK-1}e^{-2\sqrt{m_sm_l}\psi}, \quad (24)$$

where, $\widetilde{m} = \frac{\sqrt{\pi}4^{m_l-m_s+1}(m_sm_l)^{m_s}\Gamma(2m_s)\Gamma(2m_l-2m_s)}{\Gamma(m_s)\Gamma(m_l)\Gamma(m_l-m_s+\frac{1}{2})}$, $m_s = \min(m_{g_1}, m_{g_2})$ and $m_l = \max(m_{g_1}, m_{g_2})$. Furthermore, to analyze the OP of the far user for a small number of IRS elements $P^s_{out_F}$, Eqn.19 is simplified by performing mathematical operations, resulting in Eqn.25.

$$P^s_{out_F} = \int_0^{\infty} f(w)\int_0^{\infty} f(v)\int_0^{B_3} f(\psi)\,d\psi\,dv\,dw, \quad (25)$$

where,

$$B_3 = \sqrt{\frac{(2^{R_F}-1)(\rho\sigma^2_{\epsilon_{D_2}} + \rho_1 w + \rho_2 v + 1)}{\rho(a_2 - a_1(2^{R_F}-1))}}.$$

On substituting the corresponding PDF's in Eqn.25, we numerically evaluate the OP for small number of IRS elements and the results are shown and discussed in 4.2.

3.2 Uplink OP Analysis

We assume that the transmitting and receiving antennas at the BS are spatially separated. In the presence of the target, the OP of the uplink users U_1 and U_2 are expressed in Eqn.26. To analyze OP for U_1 ($P^{U_1}_{out}$), Eqn.8 is substituted into Eqn.26, yielding Eqn.27. Subsequently, by applying co-phasing and simplifying, we obtain the expression given in Eqn.28. Further, simplifying Eqn.28, we obtain Eqn.29 where, h_2, h_{LI}, and h_{ss} are denoted by x, y and q, respectively. The expression in Eqn.29 is numerically evaluated, the resulting OP of the near user at the BS is presented in Sec 4.2 and verified through simulation. Furthermore, to analyze the OP for U_2 ($P^{U_2}_{out}$), by substituting Eqn.9 into Eqn.26, Eqn.30 is obtained. Further simplifying Eqn.30, Eqn.31 is obtained and it is numerically evaluated, verified and presented in Sec 4.2.

$$P^{UL}_{out_l} = P_r(\log_2(1+\gamma_l) \le R_l), \quad (26)$$

where, $l \in [U_1, U_2]$.

$$P^{U_1}_{out} = P_r\left(\frac{|h_2|^2P_1}{P_2\left(\sum_{k=1}^{K}|g_{3k}||g_{4k}|\right)^2 + P_2\sigma^2_{\epsilon_{U_2}} + P_1\sigma^2_{\epsilon_{U_1}} + P(|h_{LI}|^2 + \delta^2|h_{SS}|^2) + \sigma^2} \le 2^{R_{U_1}} - 1\right), \quad (27)$$

$$P^{U_1}_{out} = P_r\left(|h_2|^2 \le \frac{2^{R_{U_1}}-1}{P_1}\left[P_1\sigma^2_{\epsilon_{U_1}} + P_2\left(\sum_{k=1}^{K}|g_{3k}||g_{4k}|\right)^2 + P_2\sigma^2_{\epsilon_{U_2}} + P\left(\delta^2|h_{SS}|^2 + |h_{LI}|^2\right) + \sigma^2\right]\right), \quad (28)$$

$$P^{U_1}_{out} = \int_0^{\infty} f(q)\int_0^{\infty} f(y)\int_0^{\infty} f(t)\int_0^{B_4} f(x)\,dx\,dt\,dy\,dq, \quad (29)$$

where, $B_4 = \frac{(2^{R_{U_1}}-1)[(t+\sigma^2_{\epsilon_{U_2}})\rho_2+\rho_1\sigma^2_{\epsilon_{U_1}}+(\delta^2 q+y)\rho+1]}{\rho_1}$.

$$P_{out}^{U_2} = P_r\left(\left|\sum_{k=1}^{K}|g_{3k}||g_{4k}|\right|^2 \leq \frac{(2^{R_{U_2}}-1)\left(\sigma^2_{\epsilon_{U_1}}P_1+\sigma^2_{\epsilon_{U_2}}P_2+(\delta^2|h_{SS}|^2+|h_{LI}|^2)P+\sigma^2\right)}{P_2}\right), \quad (30)$$

$$P_{out}^{U_2} = \int_0^\infty f_{|q|^2}(q)\int_0^\infty f_{|y|^2}(y)\int_0^{B_5} f_T(t)\,dt\,dy\,dq, \quad (31)$$

$$y_{BS} = \underbrace{\left(\sum_{k=1}^{K}|g_{3k}|\,|g_{4k}|+\epsilon_{U_2}\right)y_{U_2}+(h_2+\epsilon_{U_1})\,y_{U_1}}_{\text{UL Signal}} + h_{LI}\,y_s + n \quad (32)$$

$$+\underbrace{\Big(\epsilon_1(\mathbf{g_1}\mathbf{\Phi}\mathbf{g_5})(\mathbf{g_1}\mathbf{\Phi}\mathbf{g_5})+\delta\,h_{SS}+\epsilon_3\big(h_{BST}(\mathbf{g_1}\mathbf{\Phi}\mathbf{g_5})+(\mathbf{g_1}\mathbf{\Phi}\mathbf{g_5})h_{TBS}\big)\Big)y_s}_{\text{Echo Signal}}.$$

$$\Delta(y_{BS}) = \frac{f(y_{BS}\mid\mathcal{H}_1)}{f(y_{BS}\mid\mathcal{H}_0)}\underset{\mathcal{H}_0}{\overset{\mathcal{H}_1}{\gtrless}}\gamma_{\text{th}}, \quad (33)$$

$$\sigma_0^2 = P_2\Big(K(1-\epsilon)+K^2\epsilon+\sigma^2_{\epsilon_{U_2}}\Big)+P_1\Big(1+\sigma^2_{\epsilon_{U_1}}\Big)+P\sigma^2_{LI}+\sigma^2, \quad (34)$$

$$\sigma_1^2 = \sigma_0^2+2P\sigma^2_{\epsilon_1}\left(K(1-\epsilon)+K^2\epsilon+\sigma^2_{\epsilon_{U_2}}\right)^2+2\delta^2P\sigma^2_{\epsilon_2} \quad (35)$$

$$+8\sigma^2_{\epsilon_3}P\delta^2\left(K(1-\epsilon)+K^2\epsilon+\sigma^2_{\epsilon_{U_2}}\right),$$

where, $B_5 = \frac{(2^{R_{U_2}}-1)\left[\sigma^2_{\epsilon_{U_1}}\rho_1+\sigma^2_{\epsilon_{U_2}}\rho_2+(\delta^2 q+y)\rho+1\right]}{\rho_2}$.

3.3 Sensing Analysis of the target

In this section, we have derived the target detection probability for the proposed system model in the presence of UL interference. We have considered a more practical and realistic propagation environment, wherein the combined effect of both direct and IRS-assisted echoes is considered. The received signal at the BS considering UL interference and sensing signal direct from the target along with the reflected path from the IRS is given by y_{BS} and presented in Eqn.32. Where, $\mathbf{g_5}$ represent the link between the IRS and target.
Based on Eqn.32, we formulate a binary hypothesis testing framework for target detection under the null hypothesis $\mathcal{H}_0$ (absence of the target) and the alternative hypothesis $\mathcal{H}_1$ (presence of the target). By invoking the Neyman–Pearson (NP) lemma, we derive the optimal decision rule that minimizes the probability of detection and probability of false alarm . According to the NP criterion [40], the likelihood ratio test (LRT) is formulated as given in Eqn.33 where, $\Delta(y_{BS})$ denotes the likelihood ratio and γ_{th} represents the corresponding threshold value. The terms $f(y_{BS}\mid\mathcal{H}_1)$ and $f(y_{BS}\mid\mathcal{H}_0)$ denote the conditional PDFs of the received signal under the hypothesis that the target is present and absent, respectively.

$$|(y_{BS})|^2 \underset{\mathcal{H}_0}{\overset{\mathcal{H}_1}{\gtrless}} \frac{\sigma_0^2\sigma_1^2}{\sigma_1^2-\sigma_0^2}\ln\left(\frac{\sigma_1^2\gamma_{\text{th}}}{\sigma_0^2}\right). \tag{36}$$

$$PoD = P_r\left(|(y_{BS})|^2 > \frac{\sigma_0^2\sigma_1^2}{\sigma_1^2-\sigma_0^2}\ln\left(\frac{\sigma_1^2\gamma_{\text{th}}}{\sigma_0^2}\right)\middle|\,\mathcal{H}_1\right), \tag{37}$$

$$PoD = \int_{\frac{\sigma_0^2\sigma_1^2}{\sigma_1^2-\sigma_0^2}\ln\left(\frac{\sigma_1^2\gamma_{\text{th}}}{\sigma_0^2}\right)}^{\infty} f_{|(y_{BS})|^2}(x)\,dx, \tag{38}$$

$$PoD = e^{-\frac{\sigma_0^2}{\sigma_1^2-\sigma_0^2}\ln\left(\frac{\sigma_1^2\gamma_{\text{th}}}{\sigma_0^2}\right)}, \tag{39}$$

$$PoF = P_r\left(|(y_{BS})|^2 > \frac{\sigma_0^2\sigma_1^2}{\sigma_0^2-\sigma_0^2}\ln\left(\frac{\sigma_1^2\gamma_{\text{th}}}{\sigma_0^2}\right)\middle|\,\mathcal{H}_0\right), \tag{40}$$

$$PoF = e^{-\frac{\sigma_1^2}{\sigma_1^2-\sigma_0^2}\ln\left(\frac{\sigma_1^2\gamma_{\text{th}}}{\sigma_0^2}\right)}. \tag{41}$$

Further, when $\mathcal{H}_0$ is given, $y_{BS} \sim \mathcal{CN}(0,\sigma_0^2)$ and when $\mathcal{H}_1$ is given, $y_{BS} \sim \mathcal{CN}(0,\sigma_1^2)$. By applying the CLT and performing some mathematical computation, the variances σ_0^2 and σ_1^2 are obtained as given in Eqn.34. By substituting the conditional PDFs $f(y_{BS} \mid \mathcal{H}_1)$ and $f(y_{BS} \mid \mathcal{H}_0)$ into Eqn.33, Eqn.36 is obtained. where, $ln(.)$ represents natural logarithm and the received power $|(y_{BS})|^2$ follows the central chi square distribution with two degree of freedom. The probability of detection PoD according to the NP is formulated as in Eqn.37. Applying the mathematical operations along with the corresponding PDF PoD is derived and presented in Eqn.39. Furthermore, the probability of false alarm PoF is derived using the NP criterion and expressed in Eqn.41.

4 Performance Evaluation

4.1 Simulation Parameters

The derived OP expressions are validated through simulations. The simulation parameters used for validation are presented in Table 2.

4.2 Results and Discussion

Fig.2 illustrates the OP of the DL near user as a function of transmit power for different power allocation coefficients, as derived in Eqn.16.

Table 2: Simulation Parameters for Proposed System

Parameters	Values
Threshold	$R_N = R_F = 100\,\text{Kbps}$
Power coefficients	$a_1 = 0.1,\ a_2 = 0.9$
Bandwidth (BW)	$BW = 20\,\text{MHz}$
Noise figure (NF)	$5\,\text{dB}$
Noise floor (in dB)	$-174 + 10\log_{10}(BW) + NF$
BS to IRS	$m_{g_1} = 3$
IRS to D_2	$m_{g_2} = 1$
Coordinate of BS	$(0, 0)$
Coordinate of D_1	$(40, 0)$
Coordinate of D_2	$(200, 0)$
Coordinate of U_1	$(-40, 0)$
Coordinate of U_2	$(-200, 0)$
Coordinate of IRS	$(40, 10)$ and $(-40, 10)$
Penetration loss (p)	$p = 20\,\text{dB}$

The OP decreases with transmit power due to the enhanced received SNR. Additionally, higher power allocation to the near user further improves outage performance, validating the effectiveness of power-domain NOMA in the IRS-assisted ISAC-NOMA system. Fig.3 illustrates the OP performance of D_2 versus transmit power. The results show that the proposed system model significantly outperforms over the conventional NOMA-ISAC system due to the additional path gain provided

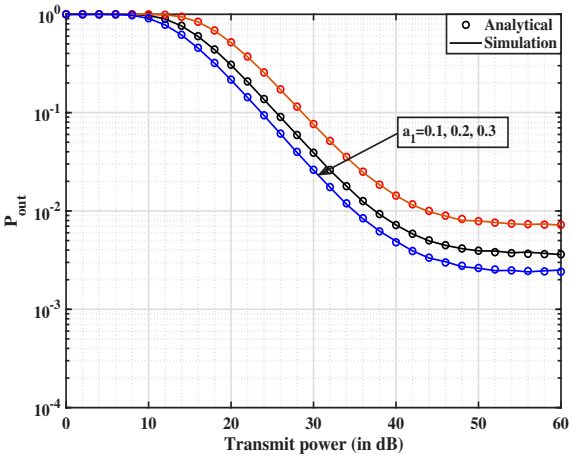


Fig. 2: OP for DL near user (D_1) versus transmit power.

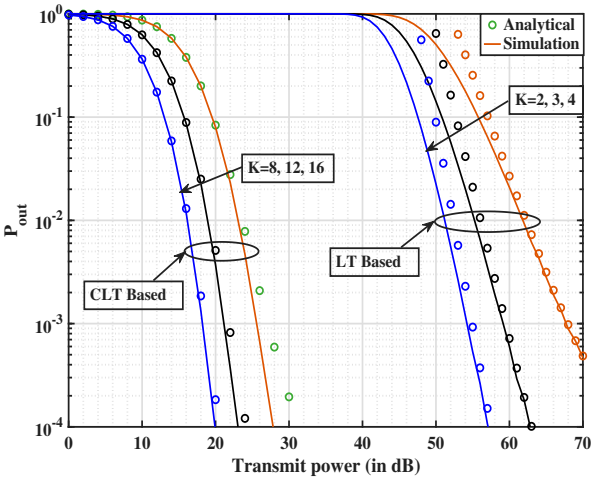


Fig. 4: OP for DL far user D_2 versus transmit power.

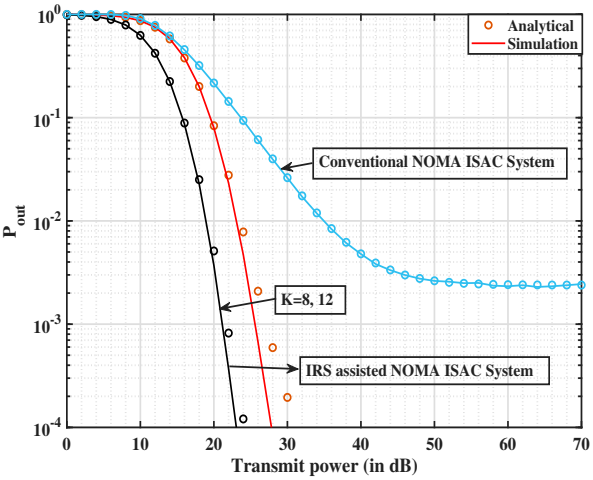


Fig. 3: OP for DL far user D_2 versus transmit power.

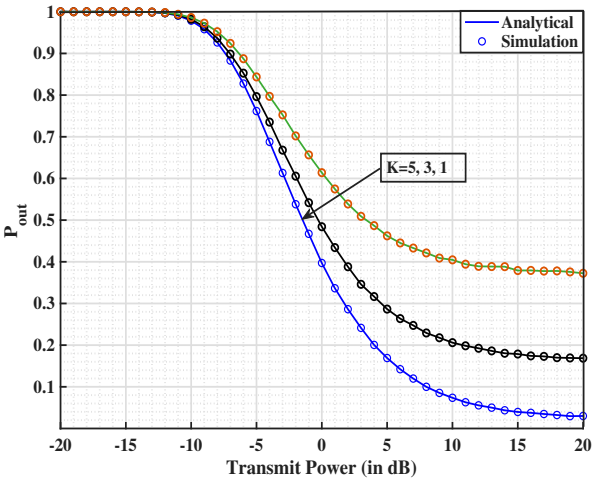


Fig. 5: OP for UL near user U_1 versus transmit power.

by passive IRS reflections. In contrast, the conventional NOMA-ISAC system exhibits performance saturation at high transmit power because of the severe interference introduced by the UL IoT devices.

Fig.4 illustrates the OP of D_2 under the UL interference, as given in Eqn.23. The OP decreases with increasing P and the figure also clearly demonstrates the benefits of the IRS elements, as the number of reflecting elements increases, the OP improves significantly. This is because the large number of IRS elements provides constructive interference at the receiver D_2 so, SNR at D_2 get improved.

Fig.5 illustrates the OP for UL near user versus transmit power for different numbers of IRS elements. From the figure, it is observed that the large K assumption based on the central limit theorem (CLT) is accurate in the low-SNR regime. However, this approximation becomes inaccurate at high SNR. To achieve accurate performance analysis in the high-SNR region, a Laplace transform (LT)–based approach is adopted, as given in (25) and also presented. The outage performance

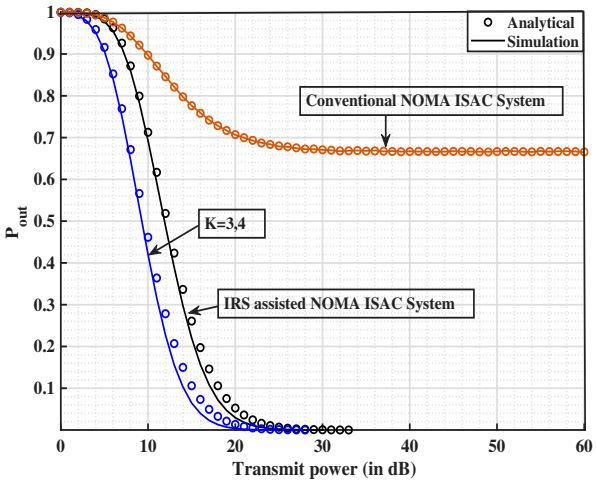


Fig. 6: OP for UL far user U_2 versus transmit power.

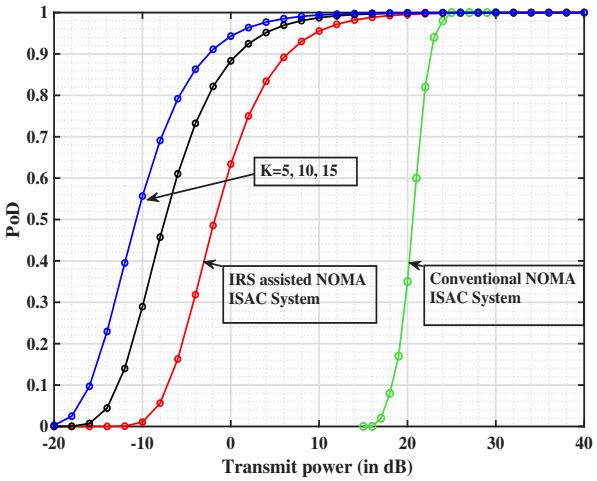


Fig. 7: PoD versus transmit power.

improves as the number of IRS elements decreases because the IRS primarily introduced to enhances the UL far-user signal, which acts as interference during near-user decoding in UL NOMA. Consequently, increasing the number of IRS elements enhances the interference from the far user, thereby degrading the near-user SINR and increasing the OP. Fig.6 illustrates the OP performance of the UL far user for small number of IRS elements (for K=3, 4) and compares the results with the conventional NOMA ISAC system. The analytical OP is numerically evaluated using Eqn.31 and the analytical and simulation results validate the accuracy of the derived expression. The OP decreases with increasing transmit power due to the improved received SNR at the BS. Moreover, the proposed system model achieves superior performance due to the passive beamforming gain provided by the IRS elements. Fig.7 illustrates the PoD versus transmit power and compares the performance with the conventional NOMA-ISAC system. The PoD is analyzed by considering the echo signal reflected through the IRS along with the UL interference. It is observed that the PoD of the conventional NOMA-ISAC system remains nearly zero for transmit power below 15 dB due to the severe interference caused by UL IoT communication signals at the BS. The proposed system model significantly improves the PoD performance by enhancing the reflected echo signal more effectively than the UL interference through IRS.

5 Conclusion

In this paper, we analyzed the reliability and sensing performance of a full duplex IRS-assisted NOMA ISAC system over Nakagami-m fading channels for future intelligent communication system. The proposed framework achieves significant improvements in terms of OP and PoD for both UL and DL transmission, thereby demonstrating its suitability for reliable wireless communication systems. By enabling intelligent propagation control through passive beamforming, IRS enhances coverage and communication reliability while reducing transmission power consumption, thereby supporting green and energy-efficient wireless transportation networks. Furthermore, the proposed framework can be further extended to unmanned aerial vehicle-assisted IRS-NOMA-ISAC architectures for dynamic and flexible coverage enhancement.

6 Declarations

Ethical Approval: In this work, no human or animal subjects were involved. Therefore, ethical approval was not required for this study.

Competing Interest: The authors declare that there are no financial or personal conflicts of interest that could have influenced the work presented in this paper.

Data availability statement: No datasets are

used in this study, as the results are obtained through analytical derivations and Monte Carlo simulations.

Funding: The authors declare that no funding was received for this research work.

Authors' Contributions: Pramod Kumar Yadav: Conceptualization, Investigation, Validation, Writing – original draft. **Sonam Jain:** Conceptualization, Reviewing and editing the manuscript, Overall supervision of this work.

References

[1] Liu, F., Cui, Y., Masouros, C., Xu, J., Han, T.X., Eldar, Y.C., Buzzi, S.: Integrated sensing and communications: Toward dual-functional wireless networks for 6g and beyond. IEEE journal on selected areas in communications **40**(6), 1728–1767 (2022)

[2] Cui, Y., Liu, F., Jing, X., Mu, J.: Integrating sensing and communications for ubiquitous iot: Applications, trends, and challenges. IEEE network **35**(5), 158–167 (2021)

[3] Mu, J., Ouyang, W., Jing, Z., Li, B., Zhang, F.: Energy-efficient interference cancellation in integrated sensing and communication scenarios. IEEE Transactions on Green Communications and Networking **7**(1), 370–378 (2023)

[4] Xiong, Y., Liu, F., Cui, Y., Yuan, W., Han, T.X., Caire, G.: On the fundamental tradeoff of integrated sensing and communications under gaussian channels. IEEE Transactions on Information Theory **69**(9), 5723–5751 (2023)

[5] Zhang, Q., Sun, H., Gao, X., Wang, X., Feng, Z.: Time-division isac enabled connected automated vehicles cooperation algorithm design and performance evaluation. IEEE Journal on Selected Areas in Communications **40**(7), 2206–2218 (2022)

[6] He, Z., Xu, W., Shen, H., Ng, D.W.K., Eldar, Y.C., You, X.: Full-duplex communication for isac: Joint beamforming and power optimization. IEEE Journal on Selected Areas in Communications **41**(9), 2920–2936 (2023)

[7] Ouyang, C., Liu, Y., Yang, H.: Performance of downlink and uplink integrated sensing and communications (isac) systems. IEEE Wireless Communications Letters **11**(9), 1850–1854 (2022)

[8] Mu, X., Wang, Z., Liu, Y.: Noma for integrating sensing and communications toward 6g: A multiple access perspective. IEEE Wireless Communications **31**(3), 316–323 (2023)

[9] Yang, Z., Xu, P., Chen, G., Wu, Y., Ding, Z.: Performance analysis of irs-assisted noma networks with randomly deployed users. IEEE Systems Journal **17**(2), 1853–1864 (2023) https://doi.org/10.1109/JSYST.2022.3195557

[10] Yadav, P.K., Jain, S., Pandey, A.: Multi-irs aided noma based iot framework for reliable and secure communication. AEU - International Journal of Electronics and Communications **203**, 156089 (2026)

[11] Yadav, P.K., Jain, S.: Outage probability analysis of irs-assisted noma system over rician fading channel. In: 2024 15th International Conference on Computing Communication and Networking Technologies (ICCCNT), pp. 1–6 (2024). https://doi.org/10.1109/ICCCNT61001.2024.10725143

[12] Jain, S., Bose, R.: Noma combined with rc for reliable and secure transmission in a delay-constrained system. IEEE Wireless Communications Letters **10**(12), 2639–2643 (2021)

[13] Van Nguyen, M.-S., Do, D.-T., Tin, P.T., Vahid, A.: Secure performance analysis of user pairs in active reconfigurable intelligent surface-aided iot systems. IEEE Systems Journal **19**(2), 370–381 (2025) https://doi.org/10.1109/JSYST.2025.3553818

[14] Hindustani, R., Dixit, D., Sharma, S., Bhatia, V.: Outage probability of multiple-irs-assisted siso wireless communications over rician fading. Physical Communication **59**, 102102 (2023)

[15] Saito, Y., Kishiyama, Y., Benjebbour, A., Nakamura, T., Li, A., Higuchi, K.: Non-orthogonal multiple access (noma) for cellular future radio access. In: 2013 IEEE 77th Vehicular Technology Conference (VTC Spring), pp. 1–5 (2013). IEEE

[16] Lin, Z., Lin, M., Wang, J.-B., De Cola, T., Wang, J.: Joint beamforming and power allocation for satellite-terrestrial integrated networks with non-orthogonal multiple access. IEEE Journal of Selected Topics in Signal Processing **13**(3), 657–670 (2019)

[17] Wang, Z., Liu, Y., Mu, X., Ding, Z., Dobre, O.A.: Noma empowered integrated sensing and communication. IEEE Communications Letters **26**(3), 677–681 (2022)

[18] Ouyang, C., Zhang, X., Liu, Y.: Performance analysis of downlink noma-isac. In: GLOBECOM 2023-2023 IEEE Global Communications Conference, pp. 7393–7398 (2023). IEEE

[19] Liu, M., Yang, M., Nallanathan, A.: On the performance of uplink and downlink integrated sensing and communication systems. In: 2022 IEEE Globecom Workshops (GC Wkshps), pp. 1236–1241 (2022). IEEE

[20] Hoang, T.M., Nguyen, B.C., Danh, N.T., Van Minh, N., Dung, L.T.: Bler and aoi analysis of multiantenna noma-fd relay systems for short-packet communications. IEEE Transactions on Reliability **75**, 738–751 (2026) https://doi.org/10.1109/TR.2026.3653652

[21] Pan, C., Ren, H., Wang, K., Kolb, J.F., Elkashlan, M., Chen, M., Di Renzo, M., Hao, Y., Wang, J., Swindlehurst, A.L., *et al.*: Reconfigurable intelligent surfaces for 6g systems: Principles, applications, and research directions. IEEE Communications Magazine **59**(6), 14–20 (2021)

[22] Yu, X., Jamali, V., Xu, D., Ng, D.W.K., Schober, R.: Smart and reconfigurable wireless communications: From irs modeling to algorithm design. IEEE Wireless Communications **28**(6), 118–125 (2022)

[23] Zhao, H., Chen, H., Li, S., Zhan, L.: Joint optimization of uav trajectory and number of reflecting elements for uav-carried irs-assisted data collection in wsns under hover priority scheme. IEEE Systems Journal **19**(3), 963–974 (2025) https://doi.org/10.1109/JSYST.2025.3607118

[24] Luo, H., Liu, R., Li, M., Liu, Y., Liu, Q.: Joint beamforming design for ris-assisted integrated sensing and communication systems. IEEE Transactions on Vehicular Technology **71**(12), 13393–13397 (2022)

[25] Huang, N., Wang, T., Wu, Y., Wu, Q., Quek, T.Q.: Integrated sensing and communication assisted mobile edge computing: An energy-efficient design via intelligent reflecting surface. IEEE Wireless Communications Letters **11**(10), 2085–2089 (2022)

[26] Zhu, Z., Li, Z., Chu, Z., Sun, G., Hao, W., Xiao, P., Lee, I.: Resource allocation for irs assisted mmwave integrated sensing and communication systems. In: ICC 2022-IEEE International Conference on Communications, pp. 2333–2338 (2022). IEEE

[27] Zhao, B., Ouyang, C., Zhang, X., Liu, Y.: Downlink and uplink noma-isac with signal alignment. IEEE Transactions on Wireless Communications **23**(10), 15322–15338 (2024) https://doi.org/10.1109/TWC.2024.3428702

[28] Singh Parihar, A., Singh, K., Bhatia, V., Li, C.-P., Ding, Z.: On performance of ris-noma assisted heterogeneous isac networks. IEEE Transactions on Cognitive Communications and Networking **12**, 3088–3103 (2026) https://doi.org/10.1109/TCCN.2025.3622346

[29] Agrawal, I., Manoj, B.R.: Ergodic rate for downlink and uplink noma aided integrated sensing and communication. IEEE Communications Letters **28**(12), 2774–2778 (2024) https://doi.org/10.1109/LCOMM.2024.3482852

[30] Xu, S., Wu, S., Guo, Y., Zheng, Y.: Ris-assisted integrated sensing and communication via full-duplex cooperative noma. IEEE

Internet of Things Journal **12**(22), 47275–47287 (2025) https://doi.org/10.1109/JIOT.2025.3600247

[31] Wei, W., Pang, X., Xing, C., Zhao, N., Niyato, D.: Star-ris aided secure noma integrated sensing and communication. IEEE Transactions on Wireless Communications **23**(9), 10712–10725 (2024) https://doi.org/10.1109/TWC.2024.3374728

[32] Raj, H., Manoj, B.: Cascaded channel statistics and target detection analysis for irs-assisted isac employing noma. In: 2025 National Conference on Communications (NCC), pp. 1–6 (2025). IEEE

[33] Wu, Q., Zhang, R.: Intelligent reflecting surface enhanced wireless network via joint active and passive beamforming. IEEE transactions on wireless communications **18**(11), 5394–5409 (2019)

[34] Islam, S.R., Avazov, N., Dobre, O.A., Kwak, K.-S.: Power-domain non-orthogonal multiple access (noma) in 5g systems: Potentials and challenges. IEEE Communications Surveys & Tutorials **19**(2), 721–742 (2016)

[35] Tang, Z., Hou, T., Liu, Y., Zhang, J., Hanzo, L.: Physical layer security of intelligent reflective surface aided noma networks. IEEE Transactions on Vehicular Technology **71**(7), 7821–7834 (2022)

[36] Gong, C., Yue, X., Wang, X., Dai, X., Zou, R., Essaaidi, M.: Intelligent reflecting surface aided secure communications for noma networks. IEEE Transactions on Vehicular Technology **71**(3), 2761–2773 (2022) https://doi.org/10.1109/TVT.2021.3129075

[37] Van, Q.-N., Nguyen, B.C., Dung, L.T., Hoang, T.M., Nguyen, H.M., Van Vinh, N., Luu, G.T.: Multiple riss for enhancing the secrecy performance of noma systems over realistic nakagami-m fading channels. IEEE Transactions on Vehicular Technology **73**(5), 6584–6599 (2024) https://doi.org/10.1109/TVT.2023.3338490

[38] Agrawal, I., Manoj, B.: Ergodic rate for downlink and uplink noma aided integrated sensing and communication. IEEE Communications Letters (2024)

[39] Cheng, Y., Li, K.H., Liu, Y., Teh, K.C., Poor, H.V.: Downlink and uplink intelligent reflecting surface aided networks: Noma and oma. IEEE Transactions on Wireless Communications **20**(6), 3988–4000 (2021)

[40] Kay, S.M.: Fundamentals of Statistical Processing, Volume 2: Detection Theory. Pearson Education India, ??? (2009)